1-2012

# Examination of the Nonlinear Dynamics of a Chaotic Acousto-optic Bragg Modulator with Feedback under Signal Encryption and Decryption

Mohammed A. Al-Saedi
*University of Dayton*

Monish Ranjan Chatterjee
*University of Dayton*, mchatterjee1@udayton.edu

Optical Engineering

SPIEDigitalLibrary.org/oe

# Examination of the nonlinear dynamics of a chaotic acousto-optic Bragg modulator with feedback under signal encryption and decryption

Mohammed Al-Saedi
Monish R. Chatterjee

SPIE

# Examination of the nonlinear dynamics of a chaotic acousto-optic Bragg modulator with feedback under signal encryption and decryption

**Mohammed Al-Saedi**
**Monish R. Chatterjee**
University of Dayton
Department of Electrical and Computer Engineering
300 College Park
Dayton, Ohio 45469
E-mail: monish.chatterjee@notes.udayton.edu.

**Abstract.** An acousto-optic Bragg cell with first-order feedback, which exhibits chaotic behavior past the threshold for bistability, was recently examined for possible chaotic encryption and recovery of simple messages (such as low-amplitude periodic signals) applied via the bias input of the sound cell driver. We carry out a thorough examination of the nonlinear dynamics of the Bragg cell under intensity feedback for (i) dc variations of the feedback gain ($\tilde{\beta}$) and the phase shift parameter ($\hat{\alpha}_0$) and (ii) ac variations of $\hat{\alpha}_{0,\text{total}}$ under signal encryption, investigating both from two different perspectives: (i) examining chaos in view of the so-called Lyapunov exponent derived recently by Ghosh and Verma and (ii) examining chaos in terms of the familiar bifurcation maps of intensity plotted against the feedback gain and the effective bias. It is shown that overall, the nonlinear dynamical results using the two approaches broadly agree, both for dc (fixed-parameter) analyses and, more importantly, when applied to the case of ac signal encryption cases. This affirms the effectiveness of the nonlinear dynamical theory in predicting and tracking the actual physical behavior of this system for message signal transmission and recovery under complex chaotic encryption.  [DOI: 10.1117/1.OE.51.1.018003]

Subject terms: Acousto-optics; hybrid A-O feedback; Bragg regime; chaotic encryption; modulation; Lyapunov exponent; bifurcation maps; chaotic bandgaps.

Paper 111240P received Oct. 5, 2011; revised manuscript received Nov. 28, 2011; accepted for publication Dec. 1, 2011; published online Feb. 6, 2012.

## 1 Introduction

Acousto-optic (A-O) bistability and chaos were first reported in the late 1970s and early 1980s by Albert et al.,[1] when it was shown that A-O devices with positive feedback gain exhibited bistability characteristics.[2] In a standard hybrid A-O feedback (HAOF) setup, a Bragg cell is driven by an ultrasonic sound wave from an RF generator (typically at 40 MHz or higher), and the resulting sound grating diffracts an incident laser beam into the first order under the Bragg condition. The first order is then picked up by a linear photodetector, fed to an amplifier, and returned to the bias input of the RF generator. The arrangement is shown in Fig. 1. Nominally, the scattered light beam is intrinsically frequency or phase modulated (with the acoustic frequency). In typical waveform sources, the external bias input amplitude modulates the RF waveform. A plot of the first-order intensity ($I_1$) versus the bias input $\hat{\alpha}_0$ yields the well-known bistable and hysteretic behavior.[2,3] It is well known that when the feedback gain or a combination of parameters is increased or adjusted sufficiently, the feedback system enters into chaos. The bistability, hysteresis, and chaotic characteristics depend strongly on the feedback gain ($\tilde{\beta}$), the feedback time delay (TD), the amplitude ($I_{\text{inc}}$) of the incident light, the initial value of the intensity ($I_1(0)$), and the effective bias voltage ($\hat{\alpha}_0$). Using the chaotic properties of the HAOF device, it was recently reported that it is possible to encrypt relatively low-bandwidth signals within the chaos wave and subsequently transmit, receive, heterodyne, filter, and recover the message signal from this chaotically encrypted carrier.[4,5] This earlier work showed a reliable and relatively robust means of secure information communication for a few simple test signals applied through the acoustic bias input. While the transmitted chaotic waves appeared to have been reasonably recovered in the test simulations, the choice of input amplitudes, frequencies, and the values of the important system parameters was based in that work primarily on studying multiple simulations and conducting tests for conditions in which chaos would appear to be fairly assured. In this paper, we examine the chaos and encryption problem from an analytic perspective in order to be able to better understand and predict the system behavior relative to the critical parameter thresholds inherent in the HAOF device. Our emphasis is on the examination of actual encryption and decryption operations seen against the predictions of two different analytic models. In Sec. 2, we present a brief background of an analytic theory based on Lyapunov exponents (LE) that lays out certain conditions under which the system either dynamically enters chaos or remains nonchaotic. This theory was developed recently by Ghosh and Verma, specifically with emphasis on the A-O system.[6] It turns out that such a dynamical system is expected to be chaotic as long as the LE is positive; it is nonchaotic otherwise. Additionally, a necessary but not sufficient condition for chaos is found to be based on a feedback gain-input optical amplitude product. A few cases are studied in Sec. 3 for the LE characteristics (with fixed values of the other parameters) involving (i) the feedback gain $\tilde{\beta}$ and (ii) the total RF driver bias voltage $\hat{\alpha}_0$. In Sec. 3.1, the dynamical behavior of the HAOF is investigated by means of so-called

0091-3286/2012/$25.00 

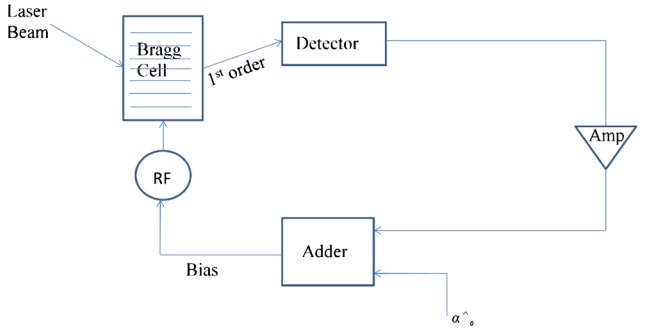


**Fig. 1** Hybrid A-O modulator with first-order feedback in the Bragg regime.

bifurcation maps—i.e., plots of the first-order intensity $I_1$ versus $\tilde{\beta}$ or $\hat{\alpha}_0$ with the values of the other parameters held constant. The results for these two approaches are shown to be generally consistent. At this stage, we need to emphasize that the results pertinent to the LE and the bifurcation maps that we present here are essentially dc characteristics along the lines of Ref. 6. We report these characteristics in order to investigate the ac encryption results against these graphs taken as templates. The aim of this paper is therefore similar to examining the ac small-signal behavior of a system on the basis of its dc bias characteristics, as is common in much of circuit theory and electronics. Since our recent work involved signal encryption and recovery using chaotic Bragg cells, it is important to examine the systems used in such chaotic modulation studies against the analytical and numerical dynamical theory developed in Secs. 3 and 3.1. Section 4 of the paper presents details of such comparisons. Overall, it is found that most of the encryption problems reported earlier generally satisfied operation of the HAOF in a stable chaotic environment, except for narrow time windows when the system was not chaotic, and hence there could not have been any signal modulation. We offer plausible explanations for such discrepancies and argue that absence of chaos over narrow windows does not affect to any large extent the overall performance of the encryption system. Section 5 concludes this paper.

## 2 Brief Background of Lyapunov Exponents Relative to the A-O Feedback System

In a recent paper, Ghosh and Verma developed an elegant analytic theory that examines the nonlinear dynamical behavior of the HAOF device (adapted for A-O) in light of the so-called Lyapunov exponent (LE) prevalent in chaos theory.[6,7] The appearance of this theory provided the impetus for the current authors to utilize it, along with standard bifurcation maps, in order to substantiate or find the behavioral limits of the ac signal encryption problem that we have studied and reported earlier.[5]

To briefly summarize the LE theory developed in Ref. 6, we first introduce the well-known intensity equation for an HAOF under feedback and delay:[6,3]

$$I_1(n\tau) = I_{\text{inc}} \sin^2\left(\frac{1}{2}\right)[\hat{\alpha}_0 + \tilde{\beta} I_1(n-1)\tau], \tag{1}$$

where $\tilde{\beta}$ is the net feedback gain, $I_{\text{inc}}$ is the intensity of the incident light beam, $\tau$ is the time delay in the feedback loop, and $n = 1, 2, 3, \ldots$ and represents the number of iterations in the feedback loop. We note next that in Eq. (1), $n\tau$ and $(n-1)\tau$ are representative of the current time and the (previous) delayed time respectively, with time (as well as the iterative cycles) being discretely repeated every $\tau$ seconds in the loop. In this respect, the integer $n$ becomes a counter for time increments (assumed in multiples of $\tau$). Hence, in what follows, the analysis is based on the integer $n$ alone (instead of $n\tau$).

Using an iterative approach, Ghosh and Verma[6] show that after $n$ iterations in the loop, the incremental change in the feedback intensity may be expressed as an exponential function, i.e.,

$$\frac{\Delta I_1}{\varepsilon} \to e^{n\lambda}, \tag{2}$$

in the limit that $n \to \infty$, and $\varepsilon \to 0$. Thus, it is clear that if the LE is positive and real ($\lambda > 0$), the iterations will arbitrarily diverge, and hence the resulting orbits will exhibit chaotic behavior (and correspondingly, chaotic time-domain oscillations, as will be shown later), whereas if $\lambda < 0$, we expect that the orbits will converge eventually to a fixed point in the trajectory plane.[3,8] Note that when the output intensity dynamically moves out of chaos, the corresponding "fixed-point" convergence implies a nonoscillating behavior in the *time domain*. Additionally, Ghosh and Verma derive a necessary but not-sufficient condition for the onset of chaos in the HAOF system, given by:

$$|\tilde{\beta} I_{\text{inc}}| > 1, \tag{3}$$

where $I_{\text{inc}}$ is the incident optical amplitude. We note that in our work, we consistently assume this amplitude to be normalized to 1. Please note that the definition of the LE (λ) as a convergent limit of a logarithmic function of the first-order intensity under feedback is derived in Ref. 6. This definition has been used in our graphical analysis.

We observe that the condition in Eq. (3), though *necessary*, may not be *sufficient* in order to ensure chaos, as has been observed by Ghosh and Verma.[6] This will be further seen from some of the results that follow.

In what follows, we examine the A-O feedback problem in terms of its dynamical behavior, specifically by looking at the LE versus appropriate system parameters (with the other parameters held constant). This will be followed by a study of the bifurcation graphs of the problem (first-order intensity versus feedback gain with other parameters held constant) and rigorously verifying the resulting chaotic and nonchaotic regimes against the aforementioned Lyapunov theory. These results are discussed in Sec. 3. We emphasize once again that the "operating point" graphs discussed in Sec. 3 (via both the LE and the bifurcation maps) are meant for use as templates for analyzing ac behavior of the HAOF system (under narrow-band small signal applications). The ac analysis results are presented in detail in Sec. 4 and constitute the primary and original work in this paper. To summarize, in the final analysis, we look further at the graphical dc "operating point" results and test the outcomes against the cases for low-frequency and low-amplitude (ac) chaotic modulation simulations that have been recently reported in the context of chaotic encryption and decryption of narrowband signals.[5]

## 3 Examination of Dynamical Behavior in Light of the Lyapunov Exponent

As mentioned, in this section we investigate the Lyapunov exponent (LE) as defined in Ref. 6 via 2-D plots of LE versus $\tilde{\beta}$ and $\hat{\alpha}_0$. For our eventual analysis for the HAOF ac encryption behavior, we remark that the LE plots versus $\hat{\alpha}_0$ are more relevant because application of ac signal occurs via the RF driver port in the HAOF device, and hence it is the $\hat{\alpha}_0$ that effectively varies under ac operation, and not the feedback gain $\tilde{\beta}$. While investigating a series of LE graphs (not shown here) versus $\tilde{\beta}$, we have found that the LE exhibits very high sensitivity with respect to several of the system dc parameters, primarily $\hat{\alpha}_0$, $I_{\text{inc}}$, and $I_1(0)$. This fact indicates that one needs to exercise great caution in selecting parameters (both dc and ac) such that a given message encryption/decryption system will operate in the chaotic regime over the entire range of the ac signal. We limit our discussion here, however, to the case of one such $\tilde{\beta}$ plot, with a fixed set of parameters that match similar parameters used in our ac encryption experiments. This plot is shown in Fig. 2, where $I_{\text{inc}} = 1$, $I_1(0) = 0$, and $\hat{\alpha}_0 = 2$. From the plot, we observe two relatively broad regions of chaos, namely a band extending from about 1.9 to 2.7, and a second one from 3.2 to 4. Within these "passbands," we see occasional negative indentations in the LE. For nomenclature purposes, we define regions of $\lambda$ where the LE is positive as *passbands* of chaos, while those regions where the LE is negative will be classified as *stopbands*. Likewise, the range of the abscissa over which the stopband extends will be defined as *chaotic bandgap*. In Fig. 3, we show the corresponding Lyapunov plot for the same $I_{\text{inc}}$ and $\hat{\alpha}_0$, but with a different initial condition, $I_1(0) = 0.25$. We observe that for the same values of the bias voltage and the incident intensity, the chaos characteristics have undergone a notable shift. Thus, the passbands now extend from about $\tilde{\beta} = 2.5$ up to $\tilde{\beta} = 4.0$, with three stopband notches around 2.8, 3.2, and 3.45. These bands are different from those in Fig. 2. These results illustrate the well-known sensitivity of chaos relative to initial conditions. We shall see later that similar sensitivity to initial conditions is also exhibited by the bifurcation maps.

As mentioned, in studying the feedback characteristics due to the LE, it turns out that examining the exponent

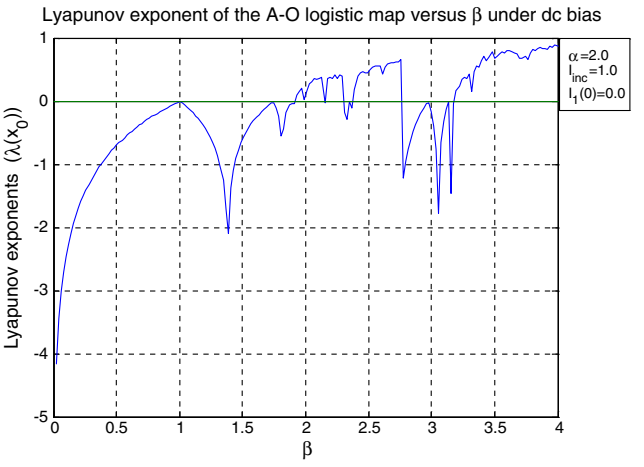


**Fig. 2** LE versus $\tilde{\beta}$ for $I_{\text{inc}} = 1$, $I_1(0) = 0$, and $\hat{\alpha}_0 = 2$.

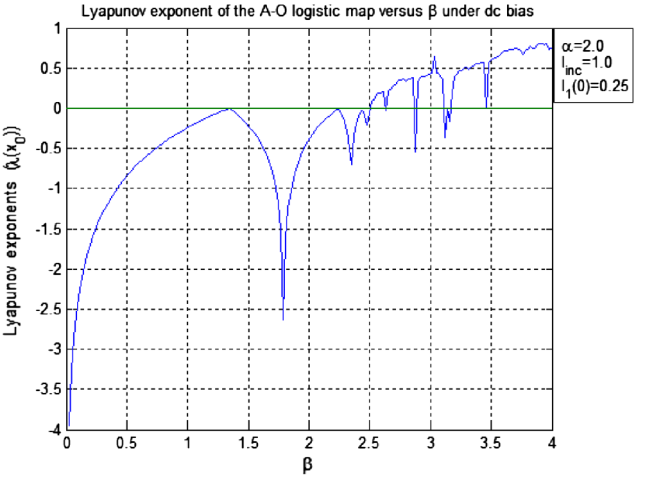


**Fig. 3** LE versus $\tilde{\beta}$ for $I_{\text{inc}} = 1$, $I_1(0) = 0.25$, and $\hat{\alpha}_0 = 2$.

relative to the acoustic driver bias ($\hat{\alpha}_0$) is more crucial to the implementation of signal modulation and encryption operations than LE versus $\tilde{\beta}$ This is because the ac signal input for the encryption operations invariably goes through the acoustic driver, and hence influences the $\hat{\alpha}_0$ behavior. We next illustrate our LE versus $\hat{\alpha}_0$ characteristics, indicating some differences vis-à-vis the corresponding dependence on $\tilde{\beta}$. The parameters corresponding to Fig. 4 showing the LE versus $\hat{\alpha}_0$ are $I_{\text{inc}} = 1$, $I_1(0) = 0$, and $\tilde{\beta} = 2$. In this case, the values correspond to the typical parameters chosen for the signal modulation/encryption simulations that we have reported elsewhere,[4,5] except to some extent that the feedback gain here is exactly one-half of that used in most of the encryption experiments. We note that with $I_{\text{inc}} = 1$ and $I_1(0) = 0$, there are only very limited passbands in the $\hat{\alpha}_0$ space where chaos happens when $\tilde{\beta} = 2$. This finding is in complete agreement with our reported modulation results, where it was seen that with $I_{\text{inc}} = 1$ and $I_1(0) = 0$, chaos occurs only when $\tilde{\beta}$ exceeds 2.41.[4,5] When $\tilde{\beta}$ is increased to 4, while keeping $I_{\text{inc}} = 1$ and $I_1(0) = 0$, we find in Fig. 5 that the chaotic bands have now increased noticeably. Thus, the LE is now positive over the bands of $\hat{\alpha}_0$ around the ranges listed in Table 1. Note that Table 1 provides a complete summary of the chaotic passbands, stopbands, and

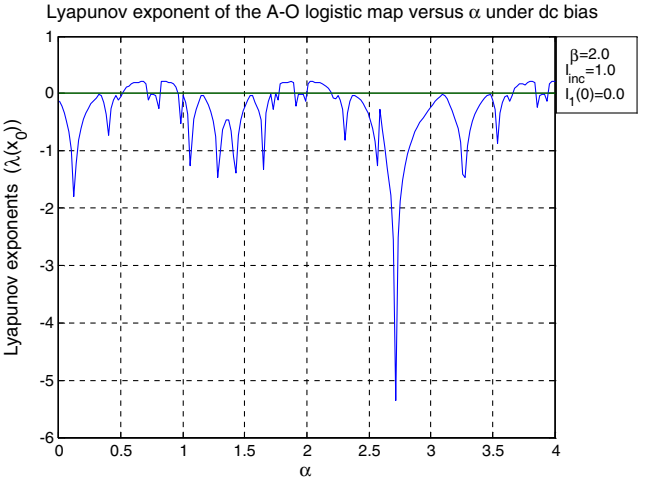


**Fig. 4** LE versus $\hat{\alpha}_0$ for $I_{\text{inc}} = 1$, $I_1(0) = 0$, and $\tilde{\beta} = 2$.

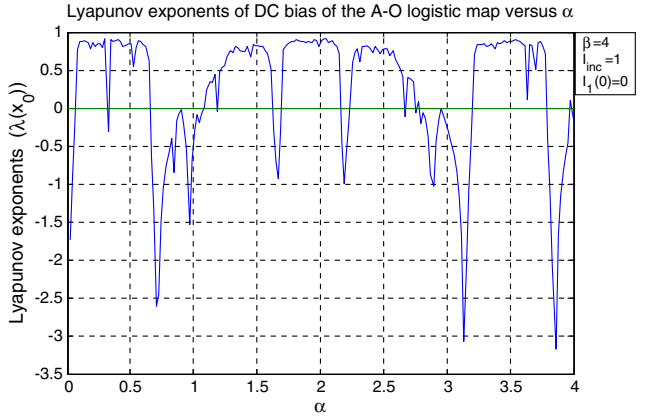


**Fig. 5** LE versus $\hat{\alpha}_0$ for $I_{\text{inc}} = 1$, $I_1(0) = 0$, and $\tilde{\beta} = 4$.

bandgaps derived from the $\hat{\alpha}_0$ plots. It is important to note that within the chaotic passbands, however, there are narrow regions where the LE becomes negative, implying nonchaotic behavior. We will further discuss the implications of these nonchaotic departures later on. We need to point out here that in the chaotic modulation work that we have reported,[4,5] a typical set of parameter values happens to be $I_{\text{inc}} = 1$, $I_1(0) = 0$, and $\tilde{\beta} = 4$. The LE characteristics illustrated by Figs. 4 and 5 clearly indicate that with $\tilde{\beta} > 3$, we expect a relatively large range of chaotic $\hat{\alpha}_0$ values. This is important for our signal processing applications, since we need to ensure chaotic operation throughout the range of (ac + dc) $\hat{\alpha}_0$ values. Overall, we observe that the sign of the LE depends critically on specific combinations of the four parameters, $\hat{\alpha}_0$, $\tilde{\beta}$, $I_1(0)$, and $I_{\text{inc}}$. Therefore, there exists a great deal of sensitivity in terms of chaotic behavior over the passbands and stopbands of these parameters, especially $\hat{\alpha}_0$ and $\tilde{\beta}$. These issues will be examined in greater detail later on, when we discuss the application of the LE to the signal encryption problem.

The nature of the Lyapunov plots presented above shows clearly that the emergence of passbands and stopbands in this complex closed-loop system is highly sensitive to both parameter values as well as initial conditions. This somewhat unstable dynamical behavior accounts for the regions of smooth transitions of $I_1$ versus $\tilde{\beta}$ in the Lyapunov plots. The results are further corroborated by the corresponding bifurcation map studies discussed next.

### 3.1 *Examination of Dynamical Behavior based on Bifurcation Maps*

In this section, we examine the dynamical behavior based on bifurcation maps of the A-O cell with feedback in the Bragg regime, with the intent to compare the resulting dynamics with those predicted by the Lyapunov theory, and to test the validity of our reported encryption/decryption results against both analyses. We first examine the first-order output intensity $I_1$ versus $\tilde{\beta}$ for fixed values of $I_{\text{inc}}$ and $I_1(0)$ with $\hat{\alpha}_0$ held constant at 2.0. One such result is shown in Fig. 6, where the value of $I_{\text{inc}}$ is set to 1, the initial condition $I_1(0)$ is set to 0 (this corresponds, incidentally, to the chaotic encryption results reported elsewhere[5]), and $\hat{\alpha}_0 = 2$. The resulting bifurcation map shows considerable differences from the case reported in Ref. 6, where $\hat{\alpha}_0$ was 2, but $I_{\text{inc}}$ and $I_1(0)$ were both held at 0.55. One notable change for this case is that the initial bifurcation (1.0 versus 1.8), the second-order bifurcation (1.75 versus 3.2), and the chaotic thresholds (2.1 versus 3.8) are all lower than the previous case; in other words, the map shifts to the left. In other words, bifurcation now starts at $\tilde{\beta} = 1$; second-order at 1.75, and steady-state chaotic behavior at about 2.1. Additionally, we observe another important dynamical feature in Fig. 6. We find that within a broad chaotic "band," say from 2 to 2.75, there emerges a narrow "forbidden band" or bandgap where the output does not exhibit chaotic oscillations. The chaotic band between 3.4 and 4, on the other hand, shows steady-state chaos. However, between 2.75 and 3.4, there is no chaos (even though there might be higher-order multistability in this range). Hence, we observe that the bifurcation maps clearly predict chaotic passbands and stopbands separated by bandgaps in the $\tilde{\beta}$ space. In comparing this finding with the LE plots discussed before, we recall that in the regions of $\tilde{\beta}$ where the LE became positive (indicating chaos), we have seen earlier how the LE undergoes negative transitions, indicating departure from chaos. Hence, both analyses predict very similar features. Examining Figs. 2 and 6, we note that we can predict non-chaotic and chaotic behavior from each diagram via different interpretations. Thus, from Fig. 2, we find that chaos happens in those windows where the LE becomes positive. We predict chaotic outputs for the case of $\hat{\alpha}_0 = 2$, $I_{\text{inc}} = 1.0$, and $I_1(0) = 0$ over the $\tilde{\beta}$ windows (or passbands) 1.9 to 2.3, 2.4 to 2.75, and 3.2 to 4.0. Likewise, Fig. 2 indicates non-chaos over the stopbands in the $\tilde{\beta}$ range 0 to 1.9, 2.3 to 2.4, and 2.75 to 3.2. From Fig. 6, on the other hand, we define chaos as the regions of the $I_1$ versus $\tilde{\beta}$ graph where we see dense, steady oscillations of the intensity in the $\tilde{\beta}$ space. By this definition, we find chaotic passbands in exactly the same regions as predicted by Fig. 2. We note further that a stopband in Fig. 6 is indicated by white bandgaps in the middle of an oscillatory waveform (the $\tilde{\beta}$. range 2.3 to 2.4, which matches the values in Fig. 2). One final note regarding the passbands has to do with the comparison of the last passbands in Figs. 2 and 6, those in the range 3.2 to 4.0. In Fig. 6, we find that the oscillations within this band do not uniformly sweep the vertical frame. Returning to the same range in Fig. 2, we find that the LE is actually positive in the entire range (thereby indicating chaos); however, in the region 3.2 to 3.3, there is a dip in the LE (i.e., the LE becomes smaller), thereby accounting for the nonuniformity in the oscillations in Fig. 6 within the same band. As was seen in Figs. 2 and 3, we also find that if the bias voltage and incident intensity are kept fixed, the chaos exhibits sizable sensitivities to small changes in the initial condition. Thus, as seen in the bifurcation map of Fig. 7, there is no unambiguous passband in the $\tilde{\beta}$.range 2.5 to 3.5 (as opposed to the clearly discernible passbands from 1.8 to 2.75 in Fig. 6), while a passband does exist from 3.6 to 4.

In contrast with Fig. 6, the dynamics of Fig. 8 (with $I_{\text{inc}} = 1$, $I_1(0) = 0.5$, and $\hat{\alpha}_0 = 1$) in the $\tilde{\beta}$ range (0 to 4) indicate a single chaotic passband, extending approximately from 3.1 through 3.6. In the region from 2.4 to 2.6, there appear to be some spurious, discontinuous oscillations, which we emphasize do not represent steady-state chaos.

Figures 9 through 11 show bifurcation maps versus the bias parameter $\hat{\alpha}_0$. In these figures, we note certain fundamental differences from the bifurcations shown earlier

versus $\tilde{\beta}$. From the figures, we once again see mono-, bi-, and multistable regions created via the serial bifurcation effect. However, in this case, we observe a tendency (perhaps more pronounced) for the "bifurcation" to proceed both ways—i.e., a single branch undergoing doubling, as well as two branches combining into one. In addition, we find that the number of chaotic passbands in the $\hat{\alpha}_0$ space (for most typical fixed values of $\tilde{\beta}$) is consistently higher than was the case in the $\tilde{\beta}$ space. Thus, in Fig. 9, with $I_{\text{inc}} = 2$, $I_1(0) = 2$, and $\tilde{\beta} = 2$, we see five passbands separated by four stopbands. Details of these bands are summarized in Table 1. We note that we have listed chaotic

**Table 1** Chaotic passbands and stopbands from bifurcation maps.

| Fixed Parameters | | | | | |
|---|---|---|---|---|---|
| $\tilde{\beta}$ | $I_{\text{inc}}$ | $I_1(0)$ | $\hat{\alpha}_0$ Passbands | $\hat{\alpha}_0$ Stopbands | Bandgaps $\Delta\alpha$ |
| 2 | 2 | 2 | 0.1 to 0.65 | 0.65 to 1.2 | 0.55 |
| | | | 1.2 to 1.55 | 1.55 to 1.65 | 0.1 |
| | | | 1.65 to 2.15 | 2.15 to 2.25 | 0.1 |
| | | | 2.25 to 2.7 | 2.7 to 3.2 | 0.5 |
| | | | 3.2 to 3.8 | 3.8 to 4.0 | 0.2 |
| 3 | 1 | 0 | — | 0 to 0.1 | 0.1 |
| | | | 0.1 to 0.65 | 0.65 to 0.7 | 0.05 |
| | | | 0.7 to 0.9 | 0.9 to 1 | 0.1 |
| | | | 1 to 1.6 | 1.6 to 3.25 | 1.65 |
| | | | 3.25 to 3.75 | 3.75 to 3.85 | 0.1 |
| | | | 3.85 to 4 | — | — |
| 3.5 | 1 | 0 | — | 0 to 0.1 | 0.1 |
| | | | 0.1 to 0.3 | 0.3 to 0.35 | 0.05 |
| | | | 0.35 to 0.85 | 0.85 to 0.9 | 0.65 |
| | | | 0.9 to 1.2 | 1.2 to 1.85 | 0.65 |
| | | | 1.85 to 2.55 | 2.55 to 3.25 | 0.7 |
| | | | 3.25 to 3.45 | 3.45 to 3.5 | 0.05 |
| | | | 3.5 to 4 | — | — |
| 4 | 1 | 0 | — | 0 to 0.1 | 0.1 |
| | | | 0.1 to 0.65 | 0.65 to 1.2 | 0.55 |
| | | | 1.2 to 1.55 | 1.55 to 1.65 | 0.1 |
| | | | 1.65 to 2.15 | 2.15 to 2.25 | 0.1 |
| | | | 2.25 to 2.7 | 2.7 to 3.2 | 0.5 |
| | | | 3.2 to 3.8 | 3.8 to 4.0 | 0.2 |
| 5 | 1 | 0 | — | 0 to 0.15 | 0.15 |
| | | | 0.15 to 0.85 | 0.85 to 0.95 | 0.1 |
| | | | 0.95 to 1.3 | 1.3 to 1.55 | 0.25 |
| | | | 1.55 to 1.9 | 1.9 to 2 | 0.1 |
| | | | 2 to 2.7 | 2.7 to 3.35 | 0.65 |
| | | | 3.35 to 4 | — | — |

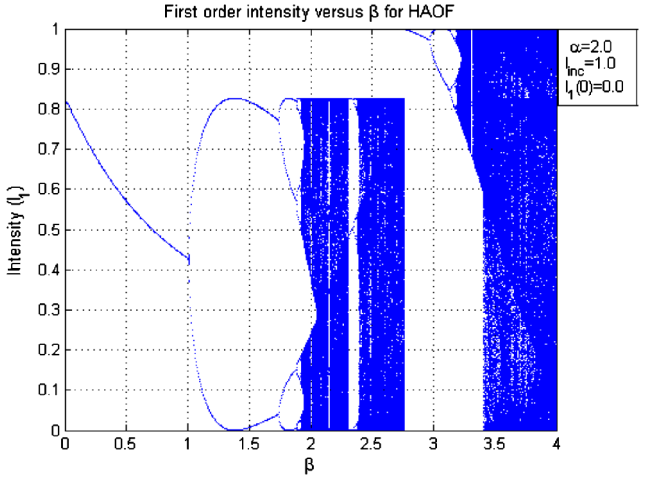


**Fig. 6** The bifurcation map of $I_1$ versus $\tilde{\beta}$ for fixed values of $I_{\text{inc}} = 1$, $I_1(0) = 0$, and $\hat{\alpha}_0 = 2$.

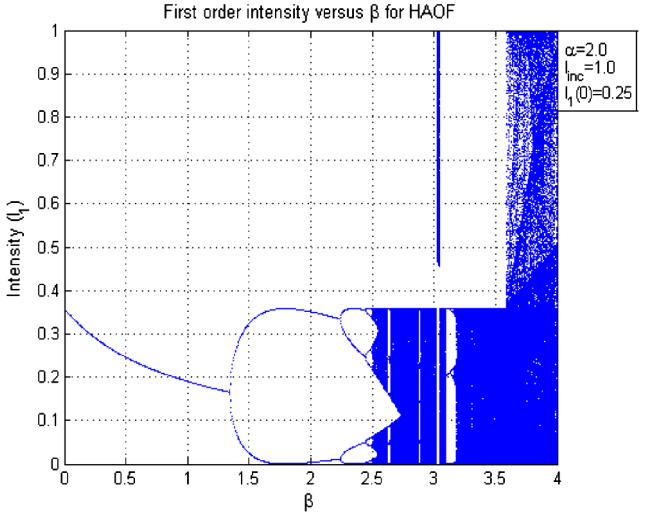


**Fig. 7** The bifurcation map of $I_1$ versus $\tilde{\beta}$ for fixed values of $I_{\text{inc}} = 1$, $I_1(0) = 0.25$, and $\hat{\alpha}_0 = 2$.

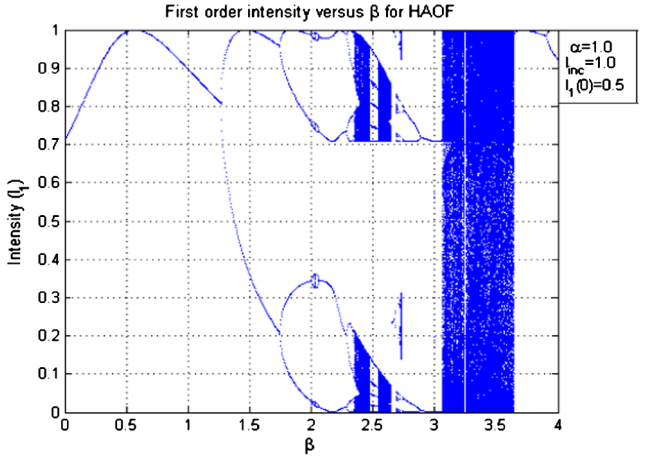


**Fig. 8** The bifurcation map of $I_1$ versus $\tilde{\beta}$ for fixed values of $I_{\text{inc}} = 1$, $I_1(0) = 0.5$, and $\hat{\alpha}_0 = 1$.

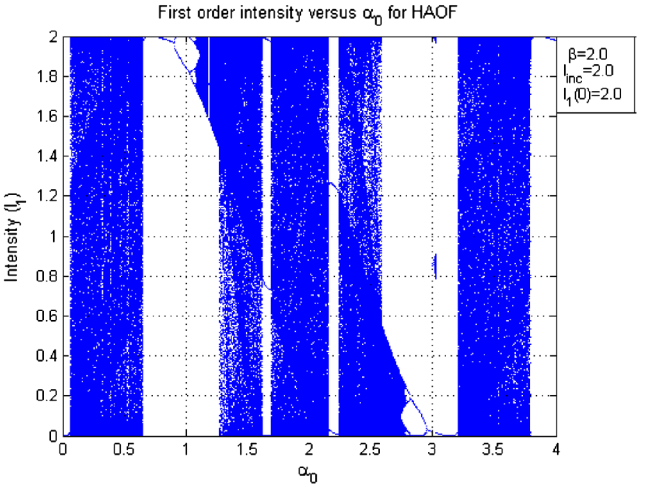


**Fig. 9** The bifurcation map of $I_1$ versus $\hat{\alpha}_0$ for fixed values of $I_{\text{inc}} = 2$, $I_1(0) = 2$, and $\tilde{\beta} = 2$.

passbands and stopbands in the $\hat{\alpha}_0$ space and not in the $\tilde{\beta}$ space, because for our signal encryption purposes, where $\hat{\alpha}_0$ varies with an ac input, the $\hat{\alpha}_0$ bands are of special interest. In Fig. 10, with $I_{\text{inc}} = 1$, $I_1(0) = 0$, and $\tilde{\beta} = 3$, we find that the overall number of passbands is essentially two in this case, one running roughly from 0.1 to 1.6 and the other from 3.25 to 4. Within these two passbands, there are very narrow stopbands (of bandgaps within 0.1), where we expect the system to be nonchaotic. The two broad passbands are also separated by a wide bandgap from 1.6 to 3.25 (bandgap = 1.65), where there is no chaos. We note also that within the large stopband, there is an area with discontinuous oscillations in the intensity (around 2.35 to 2.65) where the chaos is not steady state. Finally, in Fig. 11, with $I_{\text{inc}} = 1$, $I_1(0) = 0$, and $\tilde{\beta} = 4$, we observe five very distinct and well-defined chaotic passbands (see Table 1), separated by two broad stopbands and two minor/narrow stopbands.

We next make an important observation regarding the dependence of chaotic behavior upon two parameters in particular: $\tilde{\beta}$ and $I_{\text{inc}}$. Figures 9 and 11 show that even though they correspond to entirely different choices of $\tilde{\beta}$, $I_{\text{inc}}$, and $I_1(0)$, the overall passband and stopband behavior for

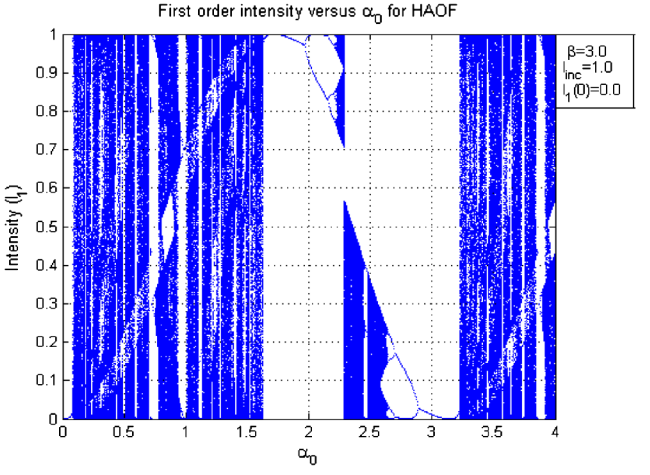


**Fig. 10** The bifurcation map of $I_1$ versus $\hat{\alpha}_0$ for fixed values of $I_{\text{inc}} = 1$, $I_1(0) = 0$, and $\tilde{\beta} = 3$.

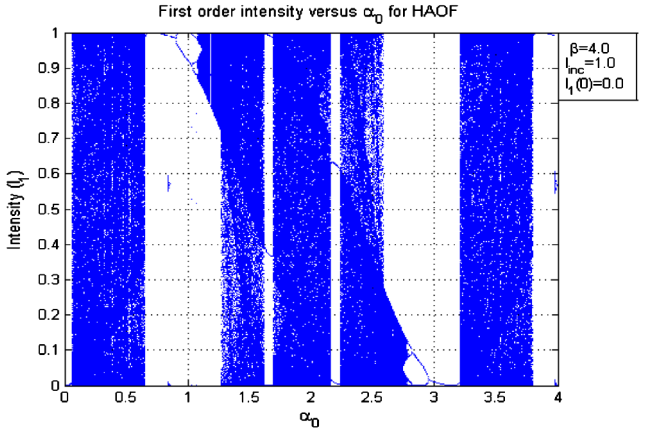


**Fig. 11** The bifurcation map of $I_1$ versus $\hat{\alpha}_0$ for fixed values of $I_{\text{inc}} = 1$, $I_1(0) = 0$, and $\tilde{\beta} = 4$.

the two cases appear to be identical for all practical purposes. This was an intriguing finding, since in general we expect stable passbands to occur at relatively higher gains. The result from Fig. 9 would tend to contradict this. We then observed that the two graphs had one feature in common: Both had the same gain-amplitude product of $|\tilde{\beta} I_{\text{inc}}| = 4.0$. This would tend to indicate that the occurrence of chaotic bands depends on the gain-amplitude product, and not necessarily on the individual values of each parameter taken separately. We have subsequently verified this hypothesis by choosing other combinations of $\tilde{\beta}$ and $I_{\text{inc}}$ such that $|\tilde{\beta} I_{\text{inc}}|$ was held constant at 4.0. The results (not shown here) showed conclusively that the chaotic band picture is invariant relative to the gain-amplitude product. Note that these results are consistent with the condition in Eq. 3. We have also found concurrently that the chaotic band picture is independent of the initial condition of the first-order light. We also note that the maximum amplitude in the bifurcation plots is determined by the value of $I_{\text{inc}}$; as a result, we find that the only distinction between Fig. 9 and Fig. 11 is in terms of the amplitude scale of $I_1$. Hence, $I_{1,\max}$ is 2 in Fig. 9 and 1 in Fig. 11. More details of these findings will be presented elsewhere.

Incidentally, some of the chaotic modulation work that we have recently reported[5] consisted of the same fixed parameter values as in Fig. 11. From Table 1, we further remark that as the value of $\beta$ is increased above 3.0 (Fig. 10), with $I_{\text{inc}} = 1$ and $I_1(0) = 0$, the chaotic bands become progressively regular, continuous, and broader. Therefore, operating an A-O feedback modulator within this range of parameters would offer greater leverage in terms of allowing larger ac amplitude variations, as well as ensuring reliable chaotic encryption within the entire passband. However, we have also seen that when $\tilde{\beta} = 2$ and $I_{\text{inc}} = 2$ (keeping the gain-amplitude product constant at 4; see Fig. 9), we have the same chaotic bands as in Fig. 11. This would potentially raise the question as to whether stable and wide-passband chaos may also be generated at lower gains by increasing the incident optical amplitude. The conclusion would appear to be in the affirmative; however, from an overall perspective, we believe that a higher feedback gain is likely to ensure that the necessary condition for chaos (Eq. 3) will be more readily satisfied. We next make one other observation regarding the "stable" chaotic passbands. Figure 11 indicates that there are five distinct chaotic passbands where the closed-loop system is undergoing stable chaotic oscillations. From a signal modulation perspective, this would require that a time-varying $\hat{\alpha}_0$ (with bias and ac inputs to the RF driver) should fall well within one of the passbands. However, we may visualize the three middle passbands in Fig. 11 as essentially one broad passband with two narrow stopbands (the white bars) in the middle. Clearly, if an effective $\hat{\alpha}_0$ is allowed to have a dynamic range corresponding to the width of this passband, then chaotic modulation will no longer occur when the $\hat{\alpha}_0$ amplitude passes over the stopbands. One would need to investigate any signal distortion or other harmful consequences of this in the encryption-decryption process. We will discuss the effect of discontinuous chaos and the resulting distortion on signal encryption in the next section.

## 4 Comparison of Lyapunov and Bifurcation Map Analyses with Chaotic Encryption and Decryption Operations

We recently reported ac signal encryption and decryption in which a number of low-bandwidth (a few kilohertz or less) ac inputs were applied to the acoustic driver bias along with a dc level shift.[5] In one such case, a 2.5-KHz sinc-function waveform was applied to the driver constrained to operate in the chaotic regime. The parameters chosen were $\tilde{\beta} = 4$, $\hat{\alpha}_{0,\text{bias}} = 2$, TD = 0.00004 sec., $I_{\text{inc}} = 1$, and $I_1(0) = 0$. The resulting chaotic waveform is shown in Fig. 12. Note that this waveform was generated by proper parameter tailoring that scrambled the time signature of the input wave from the envelope of the modulated waveform. Specifically, a periodic sinc-function waveform of unit amplitude was added to a 2 V dc bias ($\hat{\alpha}_0$) applied from the external bias/modulation input of the RF acoustic source. The ac waveform is shown in Fig. 13. Note that each cycle of the sinc function is 0.4 ms long, implying thereby a fundamental frequency of 2.5 KHz. The effective $\hat{\alpha}_{0,\text{total}}$ extends from 1.8 to 3.0 V over the time range shown. The bifurcation map corresponding to $\tilde{\beta} = 4$, $\hat{\alpha}_0 = 2$, TD = 0.00004 sec., $I_{\text{inc}} = 1$, and $I_1(0) = 0$ versus $\hat{\alpha}_0$ is the one in Fig. 11. From this figure, it is clear that the applied bias voltage falls within the stopbands (2.15 to 2.25, and 2.65 to 3.0 for the ac + dc $\hat{\alpha}_{0,\text{total}}$ in Figs. 11 and 13) of the bifurcation map. Therefore, it would appear that when the total applied bias varies in amplitude between 1.8 and 3.0 (Fig. 13), there should be no chaos in the window 2.15 to

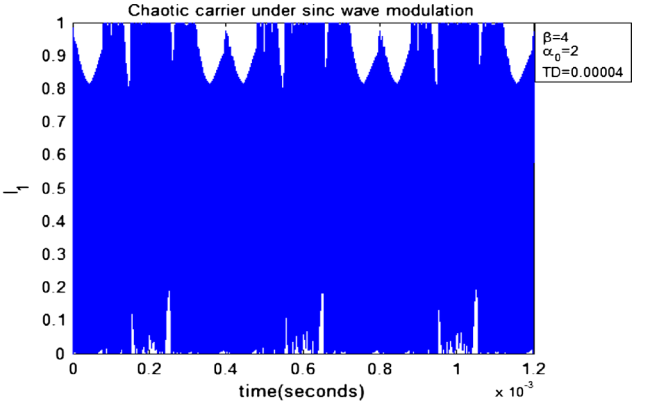


**Fig. 12** Encrypted chaotic carrier with sinc-function input for $\tilde{\beta} = 4$ and $\hat{\alpha}_0 = 2$ (see Ref. 5).

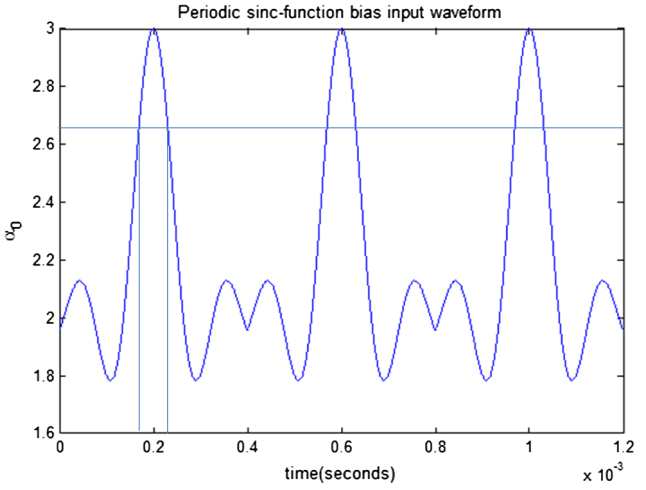


**Fig. 13** Sinc-function input wave showing nonchaotic window in time.

2.25 and weak chaos in the window 2.65 to 3.0. Next, we examine the same problem in light of the Lyapunov theory as applied to the corresponding dc-chaos case of Fig. 5. We observe from Fig. 5 that there are two nonchaotic windows within the $\hat{\alpha}_{0,\text{total}}$ range of 1.8 to 3.0. From the Lyapunov analysis, these two windows are 2.15 to 2.25 and 2.7 to 3, matching those found from the bifurcation map. Another interesting observation regarding the two dynamical analyses is as follows: From the Lyapunov graph of Fig. 5, we find that the stopband around 2.7 to 3 appears to be generally comparable to that for the stopband around 2.15 to 2.25—i.e., they both have similar negative LEs. This would nominally imply nonchaotic behavior in both bands, but slightly less in the one around 2.7 to 3.0 (since the LE transitions from less to more negative). The bifurcation map of Fig. 11 shows clearly nonchaotic behavior around 2.15 to 2.25, while there is evidence of very weak chaos around 2.7 to 3.0. Interestingly, despite these two nonchaotic and weakly chaotic windows, the overall encryption and signal recovery, as reported, seem to have worked out reasonably well, as will be discussed later. Figure 14 shows the applied sinc-function waveform and the final waveform recovered from the encrypted chaotic wave following heterodyne detection and filtering.[5] Next, note that in the weakly chaotic window (2.65 to 3.0), the sinc waveform of Fig. 13 crosses over the time range 0.176 to 0.218 ms. Intuitively, we expect that since the bifurcation nonlinear dynamics (Fig. 11) predicts at best a weak chaos in this time window, no significant chaotic oscillations should occur in the time-waveform of the first-order diffracted light from the feedback system. We have investigated the chaotic waveform for $I_1$ in the neighborhood of this time frame (0.16 to 0.24 ms) to see if this intuition is correct or not. As seen from Fig. 15, chaotic oscillations are indeed virtually absent in the modulated output waveform within the prescribed time window. This result corroborates the findings from nonlinear dynamics against the simulation results from chaotic modulation. We next remark that according to the bifurcation map of Fig. 11, there is also a second, albeit narrow stopband (2.15 to 2.25) within the $\hat{\alpha}_{0,\text{total}}$ range of 1.8 to 3.0. Transferring this information to the sinc-function waveform of Fig. 13, we find that the non-chaotic passage of the signal occurs over very narrow slices of time (on the order of less than 20 μs on each side of the symmetrical waveform). The extent of this nonchaos/nonmoldulation over the entire sinc-function period is about (20/400) or 5% in each window. As a result, as seen from the recovered waveform, its effect is minimal. We also note that the time-oscillation patterns under signal encryption will likely be significantly different from the corresponding chaotic oscillations without any ac signal present. A spectral analysis of the chaotic waveform under signal modulation will usually reveal these fundamental differences directly. Accordingly, when we carry out a fast Fourier transform of the chaotic waveform in Fig. 12 (which is a dense version of Fig. 15) under a periodic sinc-function (ac) drive applied to the acoustic source, we obtain the spectrum shown in Fig. 16. This spectrum reveals strong peaks at around 15 KHz, 12.5 KHz, 10 KHz, 7.5 KHz, 5 KHz, and others dispersed every 2.5 KHz around the center. This spectrum of the waveform[8] is clear evidence of several features of our physical system: (i) the chaos waveform under dc bias (with average chaos frequency 10.7 KHz) has been modulated by the 2.5 KHz sinc-function wave applied through the bias input; this modulation is similar to a double sideband (DSB) type amplitude modulation, with the carrier corresponding to the average chaos frequency; (ii) the slight drop or left shift in the chaotic modulated spectrum is explained by the fact that the chaotic carrier is not a deterministic sinusoidal carrier, but instead possesses small amounts of amplitude fluctuations even without any ac signal applied to the bias source, thereby resulting in a spectral

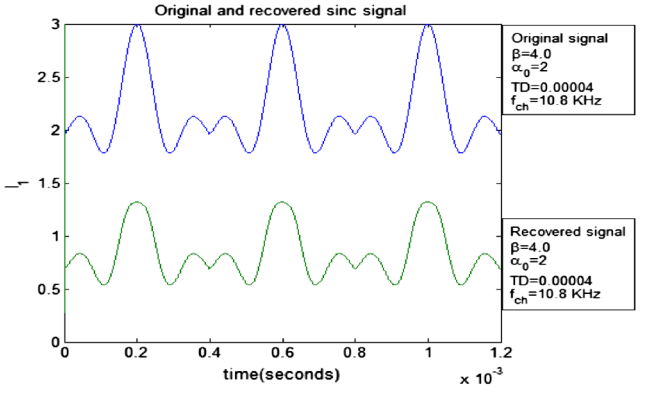


**Fig. 14** Original and recovered sinc functions under chaotic encryption and decryption (see Ref. 5).

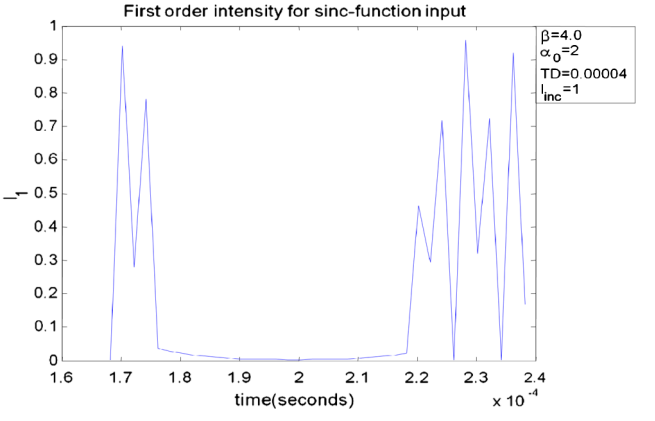


**Fig. 15** Zoomed snapshot of chaotic modulation of Fig. 14 showing absence of chaos around 0.176 to 0.218 ms.

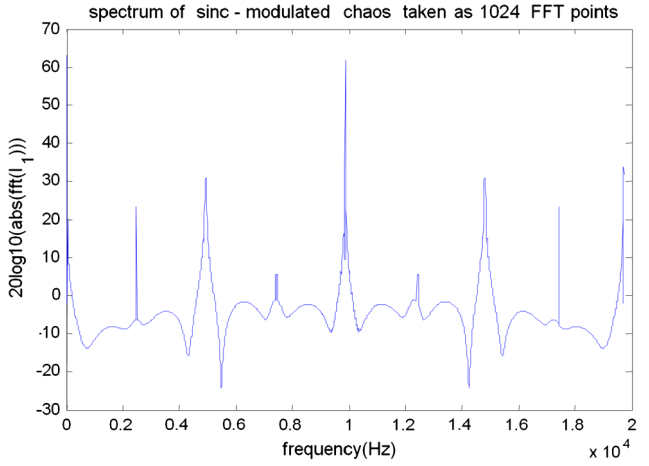


**Fig. 16** Frequency spectrum of the chaotic modulation of Fig. 14 indicating DSB-type behavior.

shift[5,9]; and (iii) a chaotic modulation phenomenon has occurred in the feedback system, even when the overall system behavior passes through narrow nonchaotic windows in time.

An additional feature of the chaotically encrypted signal transmission example being discussed here is the relative integrity of the recovered signal wave that was obtained from the modulated/encrypted chaotic carrier by means of an equivalent heterodyne detection and low-pass filtering at the receiver. This is illustrated in Fig. 14. As seen in Fig. 14, the final recovered waveform bears a reasonable resemblance (in both periodicity and amplitude profile) to the original signal wave. This result to some degree attests to the robustness of this chaotic scheme, since we have already shown that the physical system through which the input sinc-function wave passes (the top waveform in Fig. 14) possesses at least two weak-chaotic to nonchaotic windows. Consequently, as we have also shown, there is no modulation in the time windows of the sinc waveform that overlap the nonchaotic windows of the LE and bifurcation maps. Normally, one would expect this unmodulated portion of the transmitted waveform to create distortion in the recovered output. However, we find the extent of such distortion in the actual recovery to be relatively small. Intuitively, the absence of modulation over narrow time windows of the input waveform can be viewed as a form of signal clipping/clamping, as happens in electronic circuits. Therefore, upon detection/demodulation, we expect the "clamped" plateaus of the original signal to ideally emerge as flat tops; however, due to the propagation and filtering process, we find that the flat tops have actually been somewhat rounded off, thereby making the final output more closely resemble the original input. Finally, in Fig. 17 we show a 3-D view of the modulated chaotic first-order intensity versus the effective $\hat{\alpha}_{0,\text{total}}$ and $\tilde{\beta}$, corresponding to the periodic sinc-function input discussed earlier. The 3-D graph (for which we have also developed video clips [not illustrated here] for evolving values of $\hat{\alpha}_{0,\text{total}}$) shows the interdependence of both $\hat{\alpha}_{0,\text{total}}$ and $\tilde{\beta}$ in their combined effect on the complex process of chaos generation and modulation. 2-D cross-sections of Fig. 17 (say along $\hat{\alpha}_{0,\text{total}}$ for fixed values of $\tilde{\beta}$) will yield graphs similar to the LE graphs presented earlier. Thus, we find that the LE in Fig. 17 undergoes both positive and negative excursions, with the amplitudes of the negative being much higher than those of the positive excursions. These results agree with our earlier 2-D plots. In examining the 3-D plot of Fig. 17 and a similar plot for a periodic triangular input, we find that there exists a narrow ridge around $\tilde{\beta} = 3.0$ where the LE remains largely negative, implying nonchaos in this neighborhood.

## 5 Concluding Remarks

The problem of acousto-optic chaos and its application to signal modulation and recovery has been examined in terms of the nonlinear dynamical characteristics of an A-O Bragg cell with first-order feedback. Specifically, the dynamics of the system are examined in terms of (i) the Lyapunov exponent

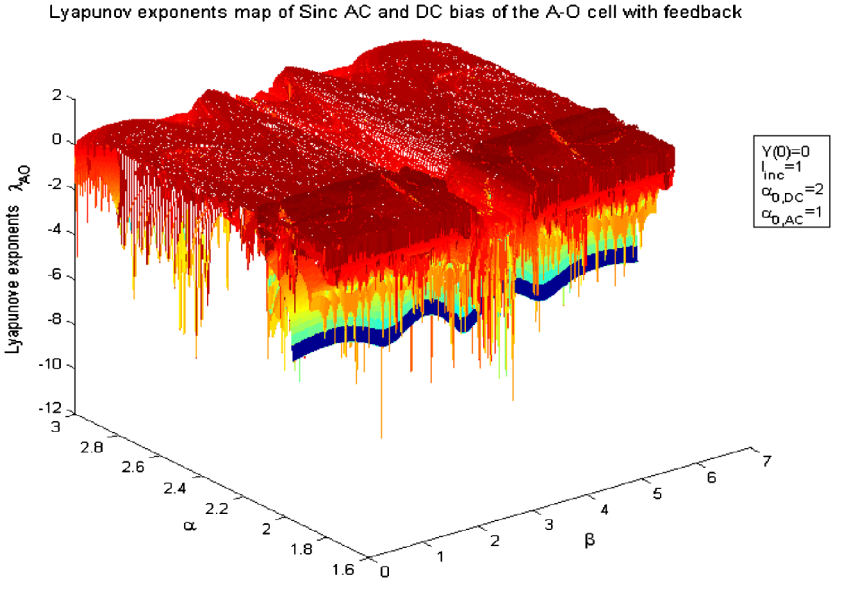


**Fig. 17** The 3-D map of Lyapunov exponents for sinc function bias input versus parameters $\tilde{\beta}$ and $\hat{\alpha}_0$ subject to initial conditions $I_{\text{inc}} = 1$ and $I_1(0) = 0$.

and (ii) the bifurcation maps. The results and conclusions are compared mutually as well as against recently reported simulation work based on low-bandwidth ac signals applied via the acoustic driver. The different approaches are shown to be generally in agreement. We remark here that our representative implementation and analysis of A-O chaos was severely limited in bandwidth (both carrier and message). Future work will involve studies with higher bandwidth and amplitude signals applied preferably to dynamical regimes where the chaotic passbands are sufficiently wide. There exists a large body of work dealing with alternative means of secure communication via chaotic encryption, several of which achieve impressively high bandwidth and data rates.[10–15] Our purpose here is not to hold up the HAOF system as a better alternative, but merely to conclusively demonstrate the feasibility of this system. It is hoped that this approach might find more practical applications (such as in medical research) in the foreseeable future.

## Acknowledgments

MAS would like to express sincere appreciation for the financial support provided by the Saudi Arabia Cultural Mission. The authors would also like to thank Professor Anjan Ghosh for suggesting and sharing the Lyapunov analysis method developed by Ghosh and Verma.

## References

1. J. Albert, R. Tremblay, and D. Vincent, "Hybrid bistable optical device using an acousto-optic waveguide modulator," *Can. J. Phys.* **59**, 1251–1253 (1981).
2. J. Chrostowski and C. Delisle, "Bistable optical switching based on Bragg diffraction," *Opt. Commun.* **41**(2), 71–74 (1982).
3. M. R. Chatterjee and J.-J. Huang, "Demonstration of acousto-optic bistability and chaos by direct nonlinear circuit modeling," *Appl. Opt.* **31** (14), 2506–2517 (1992).
4. M. Chatterjee, M. A. Alsaedi, and A. K. Ghosh, "Performance measures in acousto-optic chaotic signal encryption system subject to parametric variations and additive noise," *Proc. SPIE* **7814**, 78140D (2010).
5. M. Chatterjee and M. A. Alsaedi, "Examination of chaotic signal encryption and recovery for secure communication using hybrid acousto-optic feedback," *Opt. Eng.* **50**(5), 055002 (2011).
6. A. K. Ghosh and P. Verma, "Lyapunov exponent of chaos generated by acousto-optic modulators with feedback," *Opt. Eng.* **50**(1), 017005 (2011).
7. R. Devaney, *A First Course in Chaotic Dynamical Systems*, 1st ed., Perseus, MA (1992).
8. B. P. Lathi and Z. Ding, *Modern Digital and Analog Communication Systems*, 4th ed., Oxford, NY (2009).
9. T. Bountis, "Fundamental concepts of the theory of chaos and fractals," in *Chaos Applications in Telecommunications*, P. Stavroulakis, Ed., CRC Press, Boca Raton, FL (2006).
10. L. O. Chua, "Chua's circuit: an overview ten years later," *J. Circuits, Syst. Comput.* **4**(2), 117–159 (1994).
11. W.-K. Ling, H.-C. Lu, and H.-K. Lam, *Control of Chaos in Nonlinear Circuits and Systems*, 1st ed., World Scientific, NJ (2009).
12. J.-P. Goedgebuer, L. Larger, and H. Porte, "Optical cryptosystem based on synchronization of hyperchaos generated by a delayed feedback tunable laser diode," *Phys. Rev. Lett.* **80**(10), 2249–2252 (1998).
13. G. VanWiggeren and R. Roy, "Communicating with chaotic lasers," *Science* **279**(3), 1198–1200 (1998).
14. A. Argyris et al., "Chaos-based communications at high bit rates using commercial fiber-optic links," *Nature* **438**, 343–346 (2005).
15. R. Lavrov, M. Jacquot, and L. Larger, "Nonlocal nonlinear electro-optic phase dynamics demonstrating 10 Gb/*s* chaos communications," *IEEE J. Quant. Electron.* **46**(10), 1430–1435 (2010).

**Monish R. Chatterjee** received his BTech (honors) degree from the Indian Institute of Technology, Kharagpur, India, in 1979, and the MS and PhD degrees from the University of Iowa, Iowa City, Iowa, in 1981 and 1985, respectively. He is currently a professor of electrical and computer engineering at the University of Dayton, Dayton, Ohio. He was a faculty member in ECE at Binghamton University, State University of New York, from 1986 to 2002. He specializes in applied optics and has contributed over 100 papers to technical conferences and published about 50 papers in archival journals and conference proceedings, and numerous reference articles on science. He is also active in the field of humanities and is the author of three books of translation from his native Bengali, along with a number of chapters contributed to several literary books.

**Mohammed Al-Saedi** received his BSEE and MSEE degrees in electrical engineering from King Saud University, Riyadh, Saudi Arabia, in 1995 and 2004, respectively. He is currently completing his research for the PhD degree at the University of Dayton, Dayton, Ohio. His areas of research interest include digital communications, signal processing, and nonlinear optics. His doctoral work has resulted in one archival journal paper and several conference presentations and articles in conference proceedings.